Available online at www.sciencedirect.com
ScienceDirect
Trans. Nonferrous Met. Soc. China 22(2012) 2638−2644
Transactions of Nonferrous Metals Society of China
www.tnmsc.cn

Precipitation behavior and properties of a new high strength Al−Zn−Mg−Cu alloy

ZANG Jin-xin, ZHANG Kun, DAI Sheng-long

Beijing Institute of Aeronautical Materials, Beijing 100095, China

Received 6 September 2011; accepted 16 December 2011

Abstract: The microstructure and the associated hardness, strength and electrical conductivity of a new Al−Zn−Mg−Cu alloy during one-step ageing treatment were systematically studied. The results show that the electrical conductivity of the alloy increased continuously with increasing ageing temperature and ageing time. At the early stage of ageing, the hardness and strength of the alloy increased rapidly and then reached the peak value. When aged at 120 °C, the hardness and strength maintained at high level for a long time after the peak value. The main precipitations are GPI zones, GPII zones and metastable η' phase. GPI and GPII zones are found in the alloy after ageing for 24 h at 120 °C, which indicates that some stable GP zones can exist through the ageing process. When aged at 160 °C, the hardness and strength decreased rapidly after the peak value. The precipitation process is significantly promoted compared with that aged at 120 °C. Both GPI zones and GPII zones disappeared after ageing for 1 h at 160 °C. The main precipitates are η' phase when aged at 160 °C for 1 h. The main precipitates are η phase when the ageing time prolongs to 24 h.

Key words: Al−Zn−Mg−Cu alloy; precipitation; ageing; microstructure; hardness; strength; electrical conductivity

1 Introduction

7xxx series aluminum alloys have been widely used in aerospace industry due to their low density, high strength and low cost [1−3]. This kind of alloy is an ageing-hardening treated alloy and heat treatment processing has a great effect on its microstructures and properties [4−8].

The characterization of the precipitates is determined by the precipitation process during the ageing treatment. The precipitation is a complex process that may include several simultaneous reactions, depending on ageing conditions [9,10]. The usual precipitation sequences may be summarized as follows [11,12]: supersaturated solid solution (SSS)→GP zones→ metastable η' phase →stable η phase.

The formation of metastable precipitates has a strong effect during the nucleation of more stable phases. GP zones are generally accepted as precipitates formed at the early stage of artificial ageing. There are two types of GP zones, i.e., GPI and GPII, which have different structures [13]. Generally, either GPI or GPII zone can form as precursors to the metastable η' phase which are semi-coherent with the Al matrix. In most practical applications, the strengthening of the Al−Zn−Mg−Cu alloys relies on the formation of GP zones and η' phase precipitates [14]. Although there have been lots of work on the evolution of the precipitates, the role of GP zones on the precipitation and the strength of the alloy is less well understand. GANG and GEREZO [12] and CHEN et al [15] suggested that only GPI zones and η' phase exist in the ageing process and GPI zones serve as the precursor to metastable η' phase. However, according to work by BERG et al [13] and FAN et al [16], both GPI and GPII are found in the alloy. Therefore, the precise precipitation sequence remains to be revealed in Al−Zn−Mg−Cu alloys.

In order to optimize and control the mechanical properties of the aluminum alloy, it is necessary to understand which phases is the main precipitates at different steps of ageing treatments. Based on this, the microstructure development of different ageing processing of a new high strength Al−Zn−Mg−Cu alloy was studied. The alloy with high strength, good fracture toughness and stress corrosion resistance has been developed in recent years. The plates of the alloy have been used for upper wing skins of A380. The aim of the

Corresponding author: ZANG Jin-xin; Tel: +86-10-62496382; E-mail: apple_zjx@163.com
DOI: 10.1016/S1003-6326(11)61511-2

present work is to characterize the precipitation behavior in the new high strength Al−Zn−Mg−Cu alloy and the corresponding properties of the alloy.

2 Experimental

The composition of the studied alloy is listed in Table 1. The ingot with the diameter of 280 mm was obtained by semi-continuous casting. Then the ingot was machined to the dimensions of *d*260 mm×500 mm and hand forged to the thickness of 100 mm.

Table 1 Composition of studied alloy (mass fraction, %)

Zn	Mg	Cu	Zr+Ti	Fe	Si	Al
7.5−8.7	1.8−2.7	1.4−2.1	<0.25	<0.15	<0.12	Bal.

The samples cut from the forge were solution treated at 470 °C for 2 h and water quenched to room temperature. Immediately after quenching, the samples were aged at 120 °C and 160 °C for 48 h, respectively. After ageing treatment, tensile tests were carried out at room temperature using an Instron testing machine and hardness tests were carried out using a Brinell hardness tester. The electrical conductivity was measured with an SMP10 type conductivity meter. Three mm-diameter disks for TEM observation were punched out directly from the hardness samples which were ground down to 0.5 mm in thickness after ageing. These disks were mechanically thinned down to ~150 μm then electropolished using twin-jet with a 30% nitric acid and 70% methanol solution at −20 °C and 15 V. TEM observations were performed using an M−2000FX microscope, operating at 200 kV.

3 Results

3.1 Mechanical properties and electrical conductivity

Figure 1 shows the Brinell hardness and the conductivity of the new Al−Zn−Mg−Cu alloy during ageing at 120 °C and 160 °C for different time. The results show that the alloy has an obvious ageing strengthening effect. When the alloy is aged at 120 °C, the hardness increases significantly with increasing ageing time at the early stage, and then keeps stable at the later stage of the ageing, as shown in Fig. 1(a). The hardness of the alloy reaches the peak value after about 2 h and then decreases rapidly with increasing ageing time at 160 °C, as shown in Fig. 1(a).

The electrical conductivity increases continuously with increasing the ageing time at 120 °C and 160 °C, as shown in Fig. 1(b). The higher the ageing temperature, the higher the electrical conductivity of the alloy obtained.

Figure 2 shows the strength values of the alloy aged

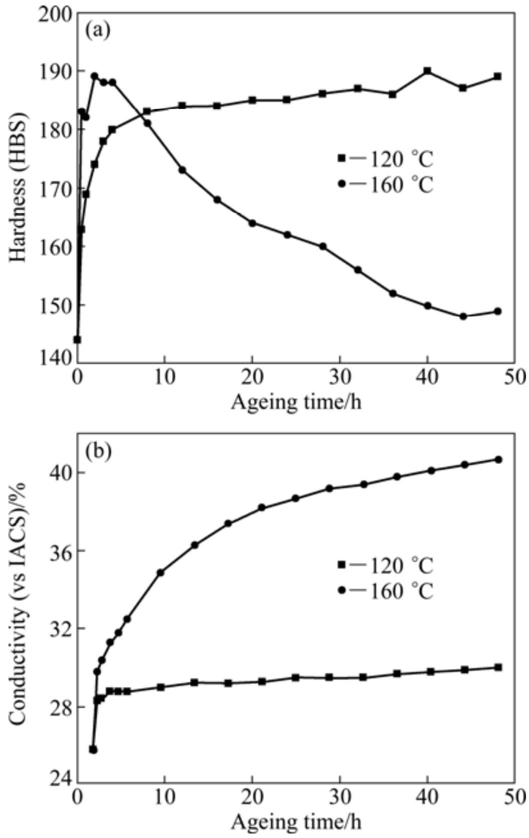

Fig. 1 Effect of ageing temperature on hardness (a) and conductivity (b) of studied alloy

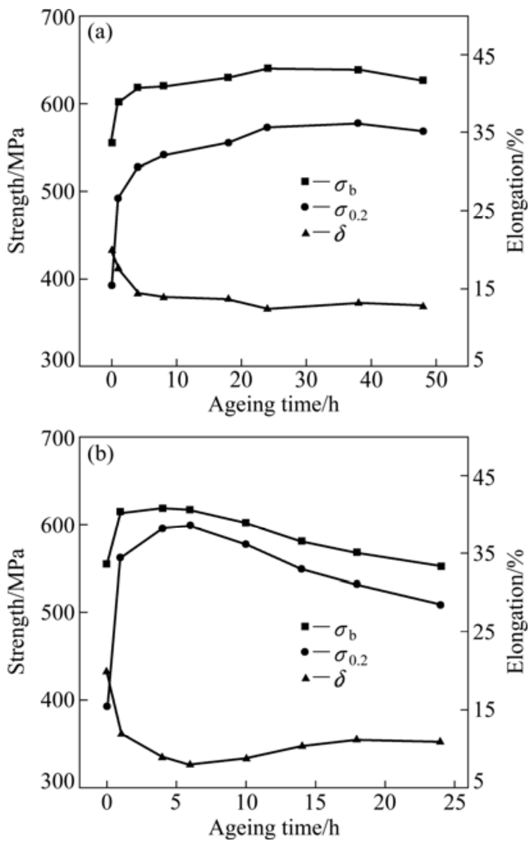

Fig. 2 Mechanical properties of alloy at different ageing temperatures: (a) 120 °C; (b) 160 °C

at 120 °C and 160 °C. The strength shows the same change tendency as the hardness shown in Fig. 1(a). The strength increases quickly at the early stage of ageing at both ageing temperatures. When aged at 120 °C, the strength reaches the peak value at 8 h, and keeps stable with increasing the time, as shown in Fig. 2(a). When aged at 120 °C for 24 h, the ultimate tensile strength, yield strength and the elongation are 640 MPa, 572 MPa and 12.5%, respectively. When aged at 160 °C for 4 h, the strength reaches the peak value and then decreases quickly, as shown in Fig. 2(b). The ultimate tensile strength, yield strength and the elongation at the peak value are 619 MPa, 596 MPa and 9%, respectively. The alloy shows extremely high strength and good elongation under both ageing conditions.

3.2 Microstructure

3.2.1 Bright field image of precipitates

Figure 3 shows the bright field TEM images near the <011> axis of Al matrix of the samples aged under different conditions. It can be seen that the precipitates distribute homogeneously in the matrix.

When aged at 120 °C, the precipitates grow slowly. After ageing at 120 °C for 1 h, darkly round

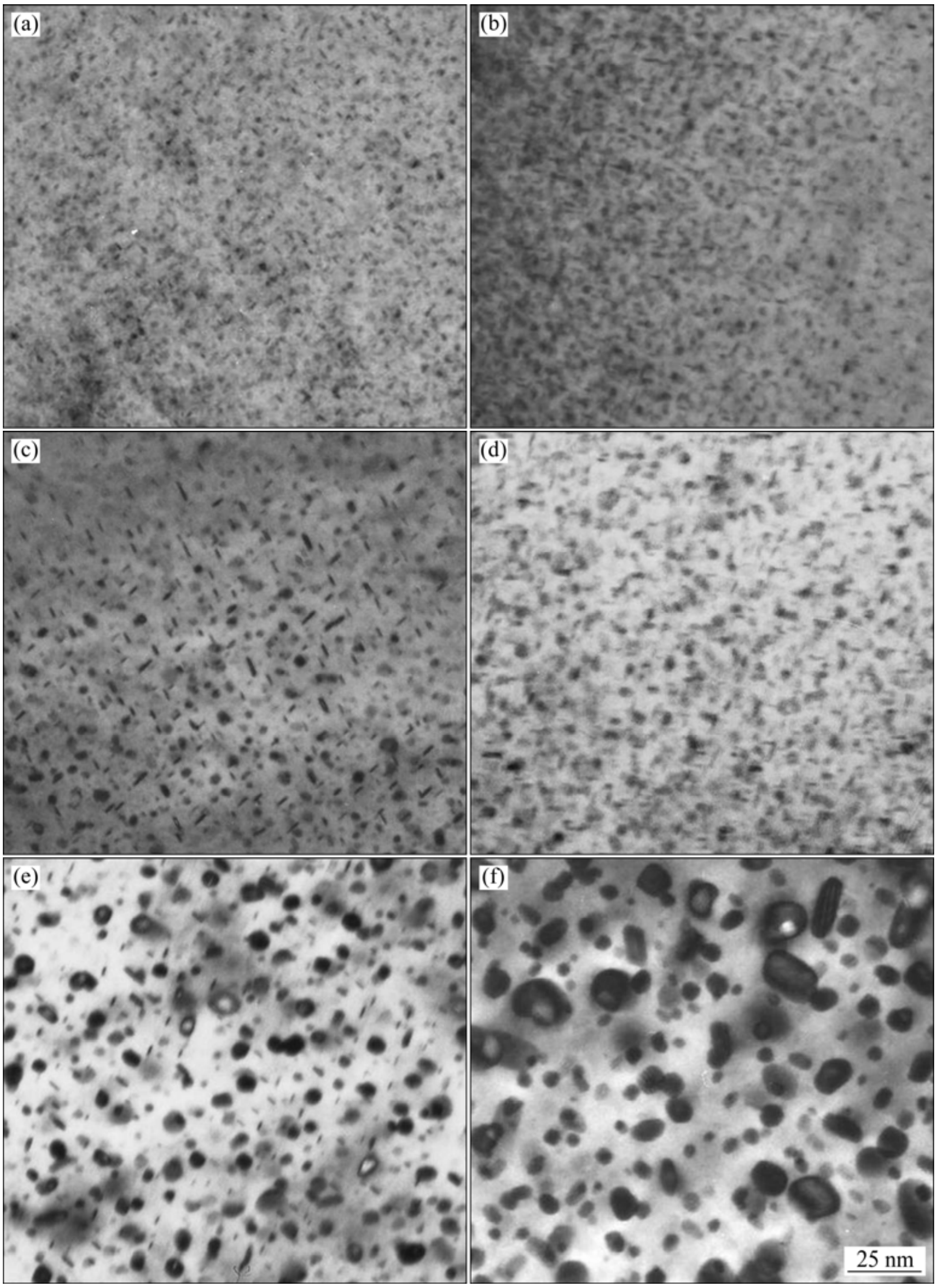

Fig. 3 Bright-field TEM images near <011> axis of Al matrix of samples aged under different conditions: (a) 120 °C, 1 h; (b) 120 °C, 4 h; (c) 120 °C, 24 h; (d) 160 °C, 1 h; (e) 160 °C, 4 h; (f) 160 °C, 24 h

precipitates with a diameter of 1−3 nm are observed in the bright field images, as shown in Fig. 3(a). Compared with ageing at 120 °C for 1 h, the size and the density of precipitates show no obvious change when aged at 120 °C for 4 h, as shown in Fig. 3(b). After ageing for 24 h at 120 °C, a lot of needle-like precipitates as well as round ones could be observed, as shown in Fig. 3(c). The sizes of needle-like precipitates are 1−2 nm in width and 3−8 nm in length.

The precipitates grow quickly when aged at 160 °C, as shown in Figs. 3(d)−(f). After ageing for 1 h, darkly round precipitates with a diameter of 3−7 nm are observed in the bright field images, as shown in Fig. 3(d). The precipitates grow to about 10 nm after ageing at 160 °C for 4 h and the density decreases, as shown in Fig. 3(e). After ageing for 24 h, the precipitates become even larger. Some small round precipitates with a diameter of 4−10 nm are randomly distributed among large rod-like precipitates (5−8 nm thick and 15−20 nm long) or blocky precipitates (20−25 nm in size), as shown in Fig. 3(f).

3.2.2 Electron diffraction analysis of precipitates

The precipitations can be identified by the selected area diffraction (SAD) patterns in different directions [12]. Figure 4 shows the SAD patterns along the directions of <001> and <112> under different ageing conditions.

Figures 4(a) and (b) show the patterns from the sample aged at 120 °C for 1 h. Diffraction spots at {1, (2*n*+1)/4, 0} in the <001> axis are observed, as shown in Fig. 4(a), which indicates the existence of GPI zones. Diffraction spots near 1/2{311} associated with the GPII zones are observed in the <112> direction, as shown in Fig. 4(b) [13]. Diffraction features of η' phases are also observed, such as diffraction spots at 1/3 {220} and 2/3 {220} positions in the <001> direction, and some diffraction spots and weak streak along {111} direction at 1/3 {220} and 2/3 {220} positions in <112> direction. After ageing at 120 °C for 24 h, there are diffraction features of GPI and GPII, as shown in Figs. 4(c) and (d). The diffraction spots of η' phase become slightly stronger in the <001> direction compared with those observed in Fig. 4(a). Strong streaks in the <112> direction are also observed in Fig. 4(d). This suggests that the volume fraction of η' phase increased after ageing for 24 h. The needle-like precipitates shown in Fig. 3(c) are mainly η' phases.

After ageing at 160 °C for 1 h, there are no obvious GPI and GPII diffraction features existing in the patterns, as shown in Figs. 4(e) and (f). There are only diffraction features of η' phases observed, such as diffraction spots at 1/3 {220} and 2/3 {220} positions in the <001> direction, and diffraction spots and streak along {111} direction at 1/3 {220} and 2/3 {220} positions in the <112> direction. After ageing at 160 °C for 24 h, the spot features of η phase become stronger and shaper further, as shown in Figs. 4(g) and (h), which indicates that the η phase is in dominant at this stage. This indicates that the rod-like precipitates and the blocky precipitates shown in Fig. 3(f) are η phases.

4 Discussion

4.1 Influence of ageing process on mechanical properties and conductivity

The hardness and strength of the alloy increase sharply at the early stage of ageing at 120 °C and 160 °C. This phenomenon can be contributed to the decomposition of the supersaturated solid solution and the formation of accelerated precipitant, as shown in Fig. 3. The whole content of alloying element is about 13%, the supersaturated degree of the matrix after solution treatment is very high and it is easier to decompose. So, the ageing response of the alloy is very sensitive. The hardness and strength reaches the peak value within 4 h at either ageing temperature.

The morphology, size and the degree of coherent with the precipitates will influence the properties of aluminum alloys [17]. When aged at 120 °C, the main precipitations are GP zones and η' phases which are small, coherent and closely spaced. And there is no obvious change in the density and the size of the particles when the ageing time prolongs to 24 h, as shown in Figs. 3(b) and (c), so the hardness and the strength of the alloy seem to be stable. When aged at 160 °C, η phase, as shown in Fig. 3(e), is one of the main precipitates, which is incoherent with the Al matrix, grows faster and coarsens further. It is known that changes of the mechanical properties are related to the particle size [18]. The rapid coarsening of the precipitates leads to high decreasing rate of hardness and strength after ageing at 160 °C 4 h.

The electrical conductivity is an effective method to indicate the stress corrosion cracking (SCC) resistance. The SCC resistance has been found to increase with increasing electrical conductivity in the Al−Zn−Mg−Cu alloy. In this work, the conductivity increases with increasing ageing temperature and ageing time, as shown in Fig. 1(b). This contributes to the continuous precipitate of GP zones, η' and η phases. According the Starink model [19], the electrical conductivity can be expressed as follows:

$$1/\sigma_{M(t)} = \rho_{M(t)} = \rho_0 + r_{Zn}x_{Zn}(t) + r_{Mg}x_{Mg}(t) \tag{1}$$

where $\sigma_{M(t)}$ is the conductivity of the matrix phase; $\rho_{M(t)}$ is the resistivity of the matrix phase; ρ_0 is the resistivity of the alloy after precipitation of the precipitation-hardening elements (Zn, Mg and Cu) has been completed; $\chi_{Zn}(t)$ and $\chi_{Mg}(t)$ are the concentrations of the Zn and Mg elements in the matrix

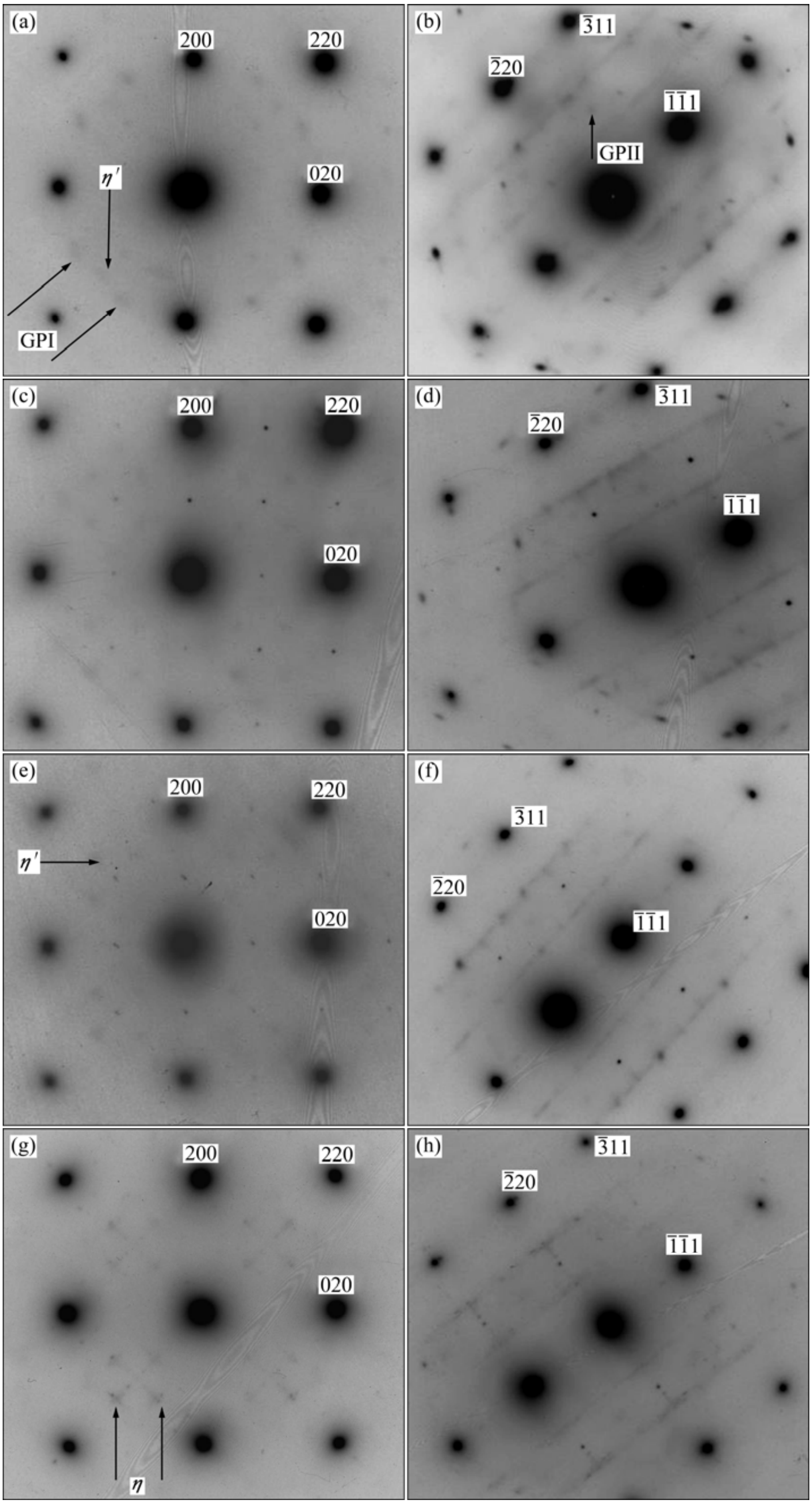

Fig. 4 SAD patterns of samples aged under different conditions: (a) (120 °C, 1 h), <001> direction; (b) (120 °C, 1 h), <112> direction; (c) (120 °C, 24 h), <001> direction; (d) (120 °C, 24 h), <112> direction; (e) (160 °C, 1 h), <001> direction; (f) (160 °C, 1 h), <112> direction; (g) (160 °C, 24 h), <001> direction; (h) (160 °C, 1 h), <112> direction

phase (which is time dependent, due to precipitation that can occur); $r_{\mathrm{Zn}}(t)$ and $r_{\mathrm{Mg}}(t)$ are constant.

The main composition of the precipitates in the alloy is $MgZn_2$. With increasing ageing time, the precipitates grow larger, so the $\chi_{\mathrm{Zn}}(t)$ and $\chi_{\mathrm{Mg}}(t)$ decrease, according to Eq. (1), the conductivity increases. It is known that the precipitation driving force increases with increasing ageing temperature [20]. At higher ageing temperature, the precipitates coarsen more rapidly than at lower ageing temperature, so the conductivity increases sharply than at lower ageing temperature. Therefore, the conductivity is higher at 160 °C than that at 120 °C at the same ageing time.

4.2 Precipitation sequence

In this study, the precipitates exhibit little change during ageing at 120 °C and 160 °C. When aged at 120 °C for 1 h to 24 h, the SAD patterns show the existence of GPI zone, GPII zone and metastable η' phases, as shown in Figs. 4(a)−(d). This shows that the main precipitates are GPI zone, GPII zone and η' phase during ageing at 120 °C. The studies show that [12] small clusters formed in the alloy immediately after quenching. These small clusters grow into lager blocky GP zones while other clusters are nucleating and growing, leading to a spread of sizes of GP zones. Both GPI and GPII zones are more unstable than η' phase and can be considered the precursors to the η' phase. During the early-stage precipitation in the alloy, direct heterogeneous nucleation of η' on large GP zones is not a dominant mechanism for η' formation. The surface energy of the smaller GP zones is higher, and they are therefore much unstable than larger GP zones. So, the smaller GP zones lead to the formation of elongated clusters and subsequently lead to the formation of η', while the larger GP zones are relatively stable and continue to grow.

It is known that the precipitation driving force increases with increasing ageing temperature [20]. Therefore, the precipitates are promoted during ageing at 160 °C and the precipitates form rapidly. In this study, when aged at 160 °C, diffraction spots associated with GP zones (GPI and GPII zones) disappeared, as shown in Figs. 4(e)−(h), which indicates that GP zones dissolved into the matrix or transformed into η' phase. The dominant precipitates are η' and η phases. It probably contributes to the higher rate of particle formation than that of particle growth at such a high ageing temperature. This suggests that some of the small GP zones dissolve and the rest transform to metastable η' phase rapidly at such high temperature [16]. After ageing at 160 °C for 1 h, the main precipitates are metastable η' phase, as shown in Figs. 4(e)−(f) and Fig. 3(d). Compared with ageing at 160 °C for 1 h, the significance feature was that the stable η precipitates with large size can be observed when aged time reaches 24 h, as shown in Fig. 3(f). This indicates that η' can be easily transformed to η at such higher temperature of 160 °C.

5 Conclusions

1) The precipitation process strongly affects the hardness, strength and the conductivity of the alloy during ageing. The hardness and strength increase significantly at the early stage of ageing at any ageing temperature due to the precipitation in the alloy. When aged at 120 °C, the hardness and strength reach peak values after ageing for 8 h and then keep stable. When aged at 160 °C, the ageing response is more quick. The hardness and strength reach the peak values after ageing for 4 h and then decrease rapidly. The conductivity increases continuously with increasing ageing temperature and aging time.

2) The precipitates in the alloy aged at 120 °C are GPI zones, GPII zones and metastable η'. Additionally, weak diffraction spots of GPI and GPII zones remained after a long time ageing (up to 24 h) at 120 °C, indicating that some stable GP zones can exist through the ageing process.

3) When aged at 160 °C, the precipitation process is significantly promoted compared with ageing at 120 °C. GP zones are not found after ageing at 160 °C for 1 h. When aged at 160 °C for 1 h, the main precipitates are η' phases. The main precipitates are η phases when the ageing time prolongs to 24 h.

References

[1] CASSADA W, LIU J, STALEY J. Aluminum alloys for aircraft structures [J]. Advanced Materials and Processes, 2002, 12: 27−29.

[2] STARK E A, STALEY J T. Application of modern aluminum alloys to aircraft [J]. Progress in Aerospace Sciences, 1996, 32(2−3): 131−172.

[3] HIRSCH J, KAHAUSEN K F, LOHTE L. Advances in industrial aluminum research and development [J]. Mater Sci Forum, 2002, 396−402: 1721−1730.

[4] SRIVATSAN T S. Microstructure, tensile properties and fracture behavior of aluminum alloy 7150 [J]. J Mater Sci, 1992, 27(17): 4772−4776.

[5] WERENSKIOLD J C, DESCHAMPS A, BRECHET Y. Characterization and modeling of precipitation kinetics in an Al−Zn−Mg alloy [J]. Mat Sci Eng A, 2000, 293(1−2): 267−274.

[6] STILLER K, WARREN P J, HANSEEN V, ANGENETE J, GJONNES J. Investigation of precipitation in Al−Zn−Mg alloy after two-step ageing treatment at 100 °C and 150 °C [J]. Mater Sci Eng A, 1999, 270(1): 55−63.

[7] WANG Tao, YIN Zhi-min, SHEN Kai, LI Jie, HUANG Ji-wu. Single-aging characteristics of 7055 aluminum alloy [J]. Transactions of Nonferrous Metals Society of China, 2007, 17: 548−552.

[8] BUHA J, LUMLEY R N, CROSKY A G. Secondary ageing in an aluminum alloy 7050 [J]. Mater Sci Eng A, 2008, 492 (1−2): 1−10.

[9] HANSEN V, STILLER K, WATERLOO G, GJONNES J, LI X Z.

Structures and transformation during artificial aging of an industrial 7xxx series Al−Zn−Mg−Zr alloy [J]. Mater Sci Forum, 2002, 396−402: 815−820.

[10] FERRGUT R, SOMOZA A, TOLLEY A. Microstructural evolution of 7012 alloy during the early stages of artificial ageing [J]. Acta Mater, 1999, 47(17): 4355−4364.

[11] LI X Z, HANSAN V, GJONNES J, WALLENBERG L R. HREM study and structure modeling of η' phase, the hardening precipitates in commercial Al−Zn−Mg alloys [J]. Acta Mater, 1999, 47(9): 2651−2659.

[12] GANG S, CEREZO A. Early-stage precipitation in Al−Zn−Mg−Cu alloy (7050) [J]. Acta Mater, 2004, 52: 4503−4516.

[13] BERG L K, GJONNES J, HANSEN V, LI X Z, KNUTSON-WEDEL M, WATERLOO G, SCHRYVERS D, WALLEBERG L R. GP zones in Al−Zn−Mg alloys and their role in artificial aging [J]. Acta Mater, 2001, 49: 3443−3451.

[14] CHINH N Q, LENDVAI J, PING D H, HONO K. The effect of Cu on mechanical and precipitation properties of Al−Zn−Mg alloys [J]. J Alloys and Compounds, 2004, 318(1−2): 52−60.

[15] CHEN Jun-zhou, ZHEN Liang, YANG Shou-jie, SHAO Wen-zhu, DAI Sheng-long. Investigation of precipitation behavior and related hardening in AA 7055 aluminum alloy [J]. Mater Sci Eng A, 2009, 500: 34−42.

[16] FAN Xi-gang, JIANG Da-ming, MENG Qin-chang, LAI Zhong-hong, ZHANG Xin-mei. Characterization of precipitation microstructure and properties of 7150 aluminum alloy [J]. Mater Sci Eng A, 2006, 427: 130−135.

[17] SEPEHRBAND P, ESMAEILI S. Application of recently developed approaches to microstructural characterization and yield strength modeling of aluminum alloy AA7030 [J]. Mater Sci Eng A, 2008, 487: 309−315.

[18] DORWARD R C, BEERNTSEN D J. Grain structure and quench-rate effects on strength and toughness of AA 7050 Al−Zn−Mg−Cu−Zr alloy plate [J]. Metall Mater Trans A, 1994, 26(9): 2481−2484.

[19] STRAINK M J, LI X M. A model for the electrical conductivity of peak-aged and overaged Al−Zn−Mg−Cu alloys [J]. Metall Mater Trans A, 2003, 34: 899−911.

[20] TANAKA H. New coarsening mechanisms for spinodal decomposition having droplet pattern in binary fluid mixture: collision- induced collisions [J]. Phys Rev Lett, 1994, 72(11): 1702−1705.

一种新型 Al−Zn−Mg−Cu 高强铝合金的析出行为及性能

臧金鑫，张 坤，戴圣龙

北京航空材料研究院，北京 100095

摘 要：对一种新型高强 Al−Zn−Mg−Cu 合金在单级时效过程中的硬度、强度、电导率变化及相应的析出行为进行系统的研究。结果表明，电导率随着时效温度的升高和时效时间的延长而不断增高。在时效开始阶段，硬度和强度随着时效的进行迅速升高并达到峰值。在 120 °C 时效时，硬度和强度到达峰值后保持稳定，主要的析出相是 GPI 区、GPII 区和 η'相。在 120 °C 长时间(直至 24 h)时效后，GPI 区和 GPII 区仍能稳定存在。在 160 °C 时效时，硬度和强度到达峰值后迅速下降。与 120 °C 时效相比，在 160 °C 时效时，析出过程更快。在 160 °C 时效 1 h 后，未观察到 GPI 区及 GPII 区的存在，主要的析出相为 η'相。在 160 °C 时效 24 h 后，主要的析出相为 η 相。

关键词：Al−Zn−Mg−Cu 合金；析出；时效；组织；硬度；强度；电导率

(Edited by YANG Hua)